Journal of Materials Chemistry C

Giant effect of spin-lattice coupling on the thermal transport in two-dimensional ferromagnetic CrI3

Journal:	*Journal of Materials Chemistry C*
Manuscript ID	TC-ART-10-2019-005928.R1
Article Type:	Paper
Date Submitted by the Author:	21-Jan-2020
Complete List of Authors:	Qin, Guangzhao; Hunan University, College of Mechanical and Vehicle Engineering Wang, Huimin; Nanjing University Zhang, Li-Chuan; University of Chinese Academy of Sciences Qin, Zhenzhen; Zhengzhou University Hu, Ming; University of South Carolina, Mechanical Engineering

Giant effect of spin-lattice coupling on the thermal transport in two-dimensional ferromagnetic CrI_3

Guangzhao Qin,[1, 2, *] Huimin Wang,[3, 1, 2, †] Lichuan Zhang,[4] Zhenzhen Qin,[5, ‡] and Ming Hu[2, §]

[1] *State Key Laboratory of Advanced Design and Manufacturing for Vehicle Body, College of Mechanical and Vehicle Engineering, Hunan University, Changsha 410082, P. R. China*

[2] *Department of Mechanical Engineering, University of South Carolina, Columbia, SC 29208, USA*

[3] *National Laboratory of Solid State Microstructures, College of Engineering and Applied Sciences, Jiangsu Key Laboratory of Artificial Functional Materials, and Collaborative Innovation Center of Advanced Microstructures, Nanjing University, Nanjing 210093, China*

[4] *Peter Grünberg Institut and Institute for Advanced Simulation, Forschungszentrum Jülich and JARA, 52425 Jülich, Germany*

[5] *School of Physics and Microelectronics, Zhengzhou University, Zhengzhou 450001, China*

High performance thermal management is of great significance to the data security and working stability of magnetic devices with broad applications from sensing to data storage and spintronics, where there would exist coupling between the spin and phonon (lattice vibrations). However, the knowledge of the spin effect on thermal transport is lacking. Here, we report that the thermal conductivity of monolayer CrI_3 is more than two orders of magnitude enhanced by the spin-lattice coupling, which has never been reported in literature. Fundamental understanding is achieved by analyzing the coupling among electronic, magnetic and phononic properties based on the orbital projected electronic structure and spin density. The bond angles and atomic positions are substantially changed due to the spin-lattice coupling, making the structure more stiff and more symmetric, which lead to the weaker phonon anharmonicity, and thus the enhanced thermal conductivity. This study uncovers the giant effect of spin-lattice coupling on the thermal transport, which would deepen our understanding on thermal transport and shed light on future research of thermal transport in magnetic materials.

The development of future digital information technology largely depends on the availability of data, which is very sensitive to the cost of data storage and thus demand- s for the increased density of data storage. During the operation of magnetic storage devices, efficient temperature control and high performance thermal management is of great significance to the data security and working stability, where thermal transport plays a key role. In particular, due to the magnetic characteristics of such devices, there would exist coupling between the spin and phonon or lattice vibrations[1]. Thus, the reliable operation of the magnetic storage device demands the fundamental study of the spin effect on the phononic thermal transport. However, despite the extensive studies on the thermal transport, the knowledge of the specific effect of spin on thermal transport is still lacking, especially for low-dimensional system[2]. Our study will fill the gap based on the study case of two-dimensional (2D) ferromagnetic chromium triiodide (CrI_3).

Since the discovery of graphene, 2D layered materials of atomic thickness have greatly attracted people's research interest with broad application prospects in many fields[3]. Very recently, 2D CrI_3 with intrinsic magnetism robustly down to monolayer limit was synthesized,[4] which shows promising applications in many technologies from sensing to data storage and spintronics[2]. Tremendous studies have been performed to explore the magnetism in 2D CrI_3, such as magnetic anisotropy,[5] lay- er thickness effect,[4,6,7] field effect,[7–9] doping,[10] strain engineering,[11] *etc*. However, the thermal transport in 2D CrI_3 has not been studied yet, which is of great significance to its applications in spintronics and magnetic storage. Most importantly, the 2D CrI_3 brings an opportunity to study the spin effect on the phononic thermal transport, which would be of great interest to the heat transfer community.

In this study, we report the giant effect of spin-lattice coupling on the thermal conductivity of monolayer CrI_3. The thermal conductivity is found more than two orders of magnitude enhanced by the spin-lattice coupling, which is especially strong for the acoustic phonon modes. Deep analysis shows that the mechanism lies in the spin-lattice coupling weakened phonon anharmonicity. This study uncovers the giant effect of spin-lattice coupling on thermal transport and the underlying mechanism, deepening our understanding on thermal transport and shedding light on future research of thermal transport in magnetic materials.

RESULTS AND DISCUSSIONS

The geometric configuration is optimized with spin [ferromagnetic (FM)] or without spin [paramagnetic (PM)] polarization, respectively. The monolayer CrI_3 possesses a much lower energy in the FM state compared to the case in the PM state, revealing the preferred stability and the FM ordering. The lattice constant, bond angles and the calculated lowest total energy of CrI_3 in FM states are found to be consistent with previous reports[12–14]. The effect of the spin-lattice coupling is firstly reflected by the structural deformation. In addi-

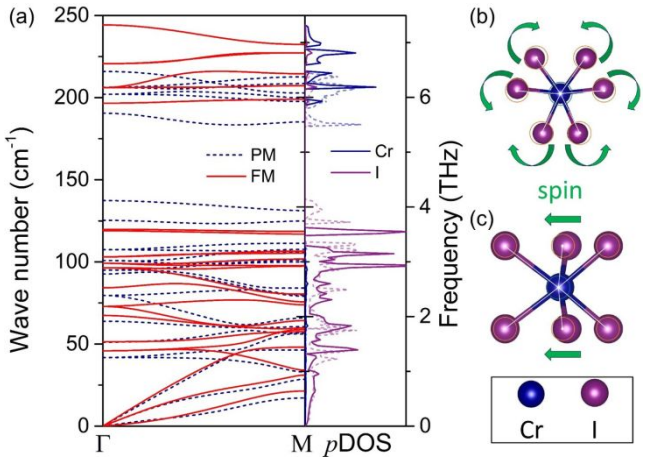

FIG. 1. The effect of spin-lattice coupling on structure and lattice vibrations of monolayer CrI_3. (a) Comparison of phonon dispersion with/without spin considered [in the ferromagnetic (FM) or paramagnetic (PM) states]. The partial density of states (*p*DOS) is calculated in the FM state. (b,c) The top and side views of monolayer CrI_3 in the PM state, where the circles, lines, and arrows show the effect of spin-lattice coupling on the geometric configuration.

tion to the lattice constant that changes from 6.992 to 7.003 A (increase by 0.158%), the bond lengths (2.3%), the bond angles, and the atomic positions change a lot, as listed in the Supplemental Table S1. Thus, the structure is altered remarkably by the spin-lattice coupling as illustrated in Fig. 1(b,c). Consequently, the structure becomes much more stiff and symmetric.

To study the effect of spin-lattice coupling on the lattice vibrations, the phonon dispersions are calculated based on the structures optimized with or without the FM ordering, respectively. As shown in Fig. 1(a), the overall group velocity for acoustic phonon branches increases slightly with FM ordering. Besides, the phonon bandgap is enlarged due to the simultaneous up- and down-shift of high- and low-frequency optical phonon modes, respectively, which is also evidently shown by the partial density of states. Thus, the spin-lattice coupling leads to the slower vibration of atom I with larger mass and the faster vibration of atom Cr with smaller mass. Note that, when we try to perform non-spin calculations based on the FM structure, imaginary frequencies emerge in the phonon spectrum, which indicates that the FM structure is not stable in the PM state without spin. Such phenomena of the imaginary frequencies also reveal the significant effect of spin-lattice coupling on the structural stability in the FM state. In addition, the FM ordering enlarged phonon bandgap also means that controlling magnetism could probably be an effec- tive and non-destructive manner to modulate the phonon bandgap beyond the strain engineering or doping[15,16].

The effect of spin-lattice coupling on the atomic vibrations governed thermal transport properties is then examined, which is characterized by the thermal conductivity. The temperature dependence of the (isotropic) thermal conductivity of monolayer CrI_3 agrees very well with the well-known $\kappa \sim 1/T$ relation. It is interesting to find the thermal conductivity having a sharp jump between the FM and PM states when the temperature reaches the Curie temperature [Fig. 2(a)]. As shown in Fig. 2(b), the thermal conductivity at room temperature (300 K) increases from 0.062 (PM state; R-TA: 0.054) to 6.599 W/m^{-1}K^{-1} (with FM ordering; R-TA: 5.437), which is a more than two orders of magnitude enhancement. Such an enhancement is rarely seen in literature[16,17]. Detailed analysis on the giant effect of spin-lattice coupling on the thermal conductivity shows that the effect is mainly on the acoustic phonon modes. The contribution to thermal transport of acoustic phonon modes increases from 32% to 88%, which becomes dominant with FM ordering [Fig. 2(b)]. The thermal conductivity with spin-lattice coupling considered is comparable to those of some typical semiconductors such as silicene (19.21 W/m^{-1}K^{-1}),[16] phosphorene (15.33 and 4.59 W/m^{-1}K^{-1} for *zigzag* and *armchair* directions, respectively),[18,19] and monolayer gallium nitride (GaN) (14.93 W/m^{-1}K^{-1})[20–22]. Thus, the thermal conductivity of monolayer CrI_3 with FM ordering would be large enough for its applications in nanoelectronics and magnetic storage. In addition, the efficient modulation of the thermal conductivity of monolayer CrI_3 promises its broad applications in thermal switch related fields, such as thermal diode, thermal transistor, thermal logic devices, *etc*.

Note that the thermal transport properties studied in this work are at room temperature (300 K), which is larger than the Curie temperature (45 K) of monolayer CrI_3[4]. As a consequence, possible manners might be needed to keep the FM ordering in monolayer CrI_3 at high temperatures [Fig. 2(a)], such as electric field,[8,9,23] magnetic field,[7] electrostatic doping,[10] *etc*. Also note that the bandgap of monolayer CrI_3 is estimated to be 1.2 eV (Fig. 4), which means that monolayer CrI3 is a semiconductor. Thus, at room temperature only the thermal conductivity contributed from phonons is considered in this study, while the contribution from electrons is neglected. In real experiments, unintentional doping would possibly happen for the exfoliated monolayer CrI_3, where the electron contribution to thermal conductivity shall be included and the results could be much more interesting that deserve further study in future.

Based on the phonon gas model and kinetic theory, the thermal conductivity (κ) can be expressed as[24]

$$\kappa_\alpha = \sum_{\vec{q}p} C v(\vec{q}, p) v_\alpha(\vec{q}p)^2 \tau(\vec{q},p), \quad (1)$$

where C_V is the volumetric specific heat capacity of phonon following the Bose-Einstein statistics, $v_\alpha(\vec{q}, p)$ is the $\alpha(= x, y, z)$ component of group velocity of phonon mode with wave vector $\vec{q}$ and polarization p, and τ is the phonon relaxation time. Based on the phonon dispersion as shown in Fig. 1(a), the heat capacity and group veloc-

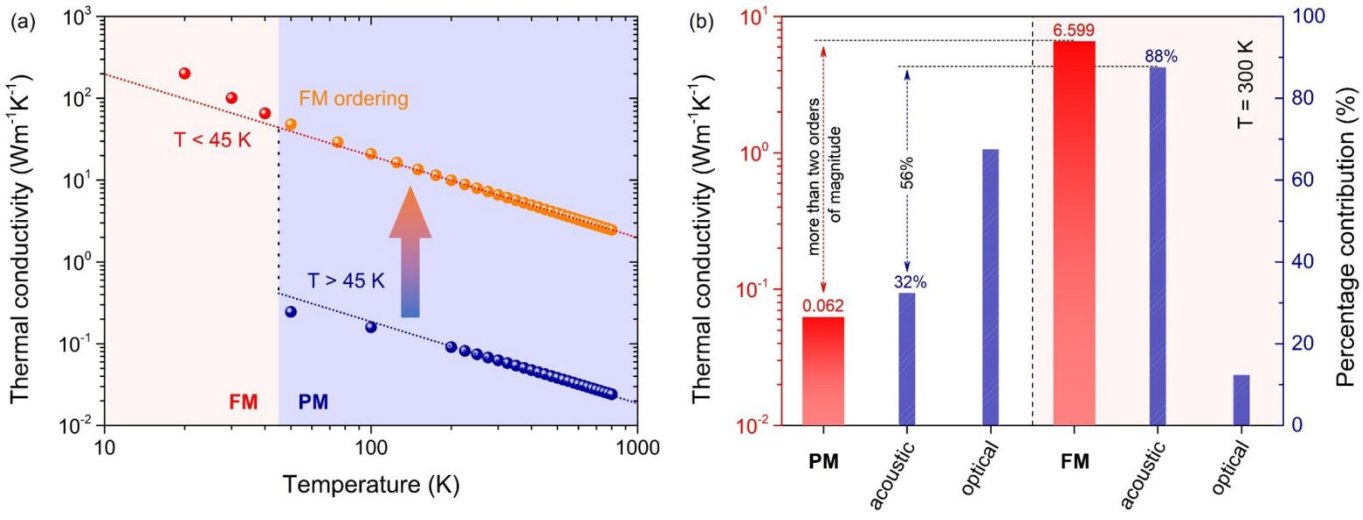

FIG. 2. The effect of spin-lattice coupling on the thermal conductivity (κ) of monolayer CrI_3. (a) The temperature dependence of κ in FM and PM states, respectively. The Curie temperature of monolayer CrI_3 is 45 K. Filled circles are from calculations and the doted lines show the $\kappa \sim 1/T$ relation. (b) The effect of spin-lattice coupling on the κ of monolayer CrI_3 by comparing the κ at 300 K between the states with/without FM ordering. The effect on the percentage contribution of acoustic and optical phonon modes to thermal transport is shown in blue referring to the vertical axis at right.

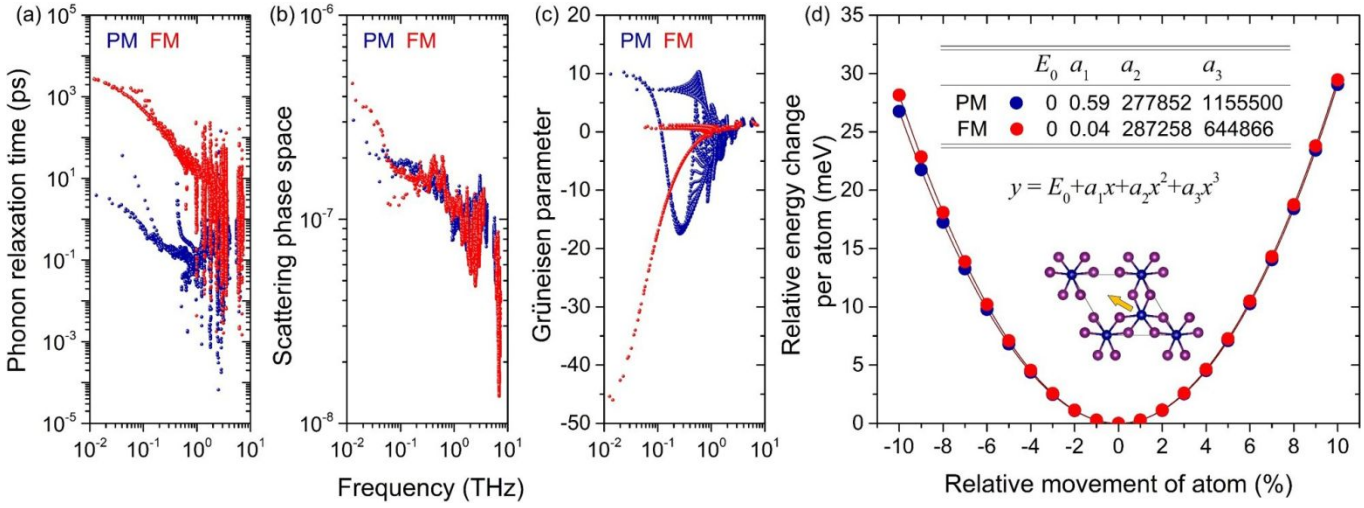

FIG. 3. Mode level analysis of thermal transport properties and anharmonicity of monolayer CrI_3. The comparison of (a) phonon relaxation time, (b) scattering phase space and (c) Grüneisen parameter with/without FM ordering. (d) The comparison of potential energy well with/without FM ordering. The inset table of (d) shows the fitted harmonic and anharmonic parameters in the inset formula. The arrow on the inset top view of the structure indicates the positive direction of atomic displacements.

ity are only altered slightly by the spin-lattice coupling. Thus, to achieve a more detailed understanding of the giant effect of spin-lattice coupling on the thermal conductivity, we further performed the mode level analysis on the phonon relaxation time [Eq. (1)].

The effect of spin-lattice coupling on the phonon relaxation time is shown in Fig. 3(a). The more than two orders of magnitude enlarged phonon relaxation time reveals the weakened phonon-phonon scattering and leads to the giantly enhanced thermal transport (Fig. 2). Specifically, the effect of spin-lattice coupling on phonon relaxation time is more remarkable for acoustic phonon modes [Fig. 3(a)], leading to its dominant role in thermal transport with FM ordering (Fig. 2) as analyzed above. It is well known that the phonon-phonon scattering is governed by two factors, namely scattering possibility and scattering strength, which are determined by scattering phase space and phonon anharmonicity, respectively. The 3-phononos scattering phase space is evaluated based on the conservation of energy and momentum of the involved phonon modes. As shown in Fig. 1(a), the phonon bandgap is enlarged by the spin-lattice coupling,

which is supposed to limit the acoustic-optical phonon scattering based on previous studies[25,26]. Consequently, the scattering phase space is slightly diminished by the spin-lattice coupling [Fig. 3(b)]. However, the alternation of the scattering phase space only changes slightly, which cannot fully explain the largely diminished scattering rate. Thus, the reason for the spin-lattice coupling weakened phonon-phonon scattering must lie in the weakened phonon anharmonicity, which is evidently shown in Fig. 3(c) as quantified by the Grüneisen parameter.

The potential energy well is plotted in Fig. 3(d) to present a visualized view of the effect of spin-lattice coupling on phonon anharmonicity by comparing the potential energy well of monolayer CrI_3 with and without FM ordering. It is shown that the corresponding energies for the positive and negative movement of atom become closer when changing from PM to FM state. Thus, the potential energy well becomes more symmetric with FM ordering. By fitting the potential energy well with a polynomial, the harmonic (a_2) and anharmonic parameters (a_3) can be obtained as listed in the inset table of Fig. 3(d). The slightly enlarged a_2 well reveals the slightly enhanced bonding strength[18,22] and the correspondingly enhanced group velocity [Fig. 1(a)]. While the largely reduced a_3 well reveals the largely weakened phonon anharmonicity as quantified by the Grüneisen parameter [Fig. 3(c)]. Moreover, the magnitude of the anharmonic IFCs is also compared between the FM and PM states. It is shown that the anharmonic IFCs for PM phase is larger than that for FM phase, which is consistent with the behavior of the phonon anharmonicity and thermal conductivity (Supplemental Figure S1).

To achieve the fundamental understanding on the underlying mechanism of the spin-lattice coupling and its effect on phonon anharmonicity, we further studied the orbital projected density of states (*p*DOS) of the electronic structure with spin and the spin density. The calculated spin-polarized electronic band structures of CrI_3 in FM states (Supplemental Fig. S3) are well consistent with previous reports[13,14]. As shown in Fig. 4(a), the total DOS for spin-up and spin-down are non-symmetric, especially near the Fermi level. Thus, there is a net magnetic moment (5.628 μ_B) in monolayer CrI_3, showing the magnetism. Detailed analysis finds that the net magnetic moment in monolayer CrI_3 mainly comes from the Cr atom. The magnetic moment on each Cr atom is 3.044 μ_B, which mainly comes from the Cr-*d* orbital (97.668%). Based on the crystal field theory, the *d* orbitals can be splitted into two groups of $d_{xy;yz;zx}(t_{2g})$ and $d_{x^2-y^2;z^2}(e_g)$. As shown in Fig. 4(b), the Cr-t_{2g} dominates the contributions at both the valence band maximum (VBM) and the conduction band minimum (CBM), which is due to the octahedral-like nature of Cr coordinates[27,28]. In addition to the Cr-*d* orbital, small contribution to the magnetic moment also comes from the I atom, which is opposite to that from the Cr atom. The magnetic moment on each I atom is 0.077 μ_B, which

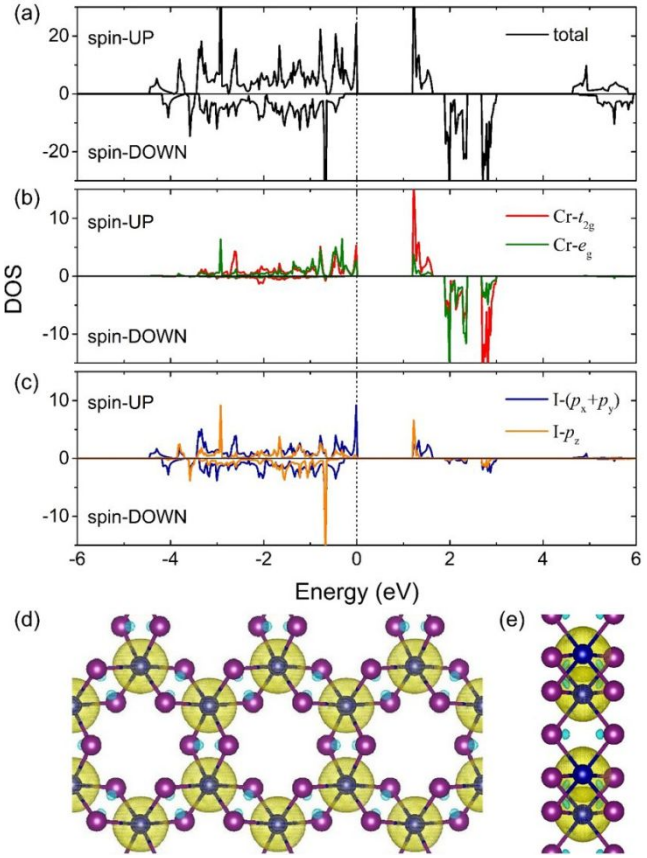

FIG. 4. The electronic projected density of states (*p*DOS) for monolayer CrI_3 with FM ordering. The (a) total *p*DOS, (b) Cr-t_{2g}, e_g orbitals projected *p*DOS, and (c) I-p_x, p_y, p_z orbitals projected *p*DOS are shown separately. (d,e) The isosurface plots (0.0045 e/A^3) for spin density with yellow indicating spin-up and cyan indicating spin-down.

mainly comes from the I-*p* orbital due to the hybridization between Cr-*d* and I-*p* orbitals. Detailed analysis based on Fig. 4(c) shows that the I-p_x, p_y dominates the contributions at the VBM while the I-p_z dominates the contributions at the CBM.

There exists strong Cr-Cr direct exchange due to the cation-cation coupling and the relatively lower energy of the Cr-t_{2g} orbital than the Cr-e_g orbital. Besides, there also exists Cr-I-Cr superexchange interaction due to the overlap between Cr-*d* and I-*p* orbitals, leading to the opposite and small contribution to the magnetic moment from *p* orbital of I atom. The magnetism in monolayer CrI_3 obtained in this work agrees very well with previous studies[29,30]. The Heisenberg exchange interactions in monolayer CrI_3 can be expressed as[1]

$$H = -\sum_{i \neq j} J_{ij} \hat{S}_i \hat{S}_j, \qquad (2)$$

where $\hat{S}_i$ is the spin state of lattice position *i*, and J_{ij} describes the exchange interactions between lattice positions of *i* and *j*. The exchange interactions directly affect the lattice vibrations by affecting the forces acting

on atoms through the effect on the Hamiltonian of the system [Eq. (2)],[1] which is evidently shown by the spin density [Fig. 4(d,e)]. Thus, the exchange interactions in monolayer CrI_3 lower the total energy of the system by 3.11 eV and make the structure more symmetric through spin-lattice coupling [Fig. 1(b,c)]. Moreover, due to the small split energy between the Cr-t_{2g} and Cr-e_g orbitals caused by the weak-field from ligand I atoms, high-spin complexes are formed in monolayer CrI_3, leading to a stronger repulsion between Cr and I atoms[27]. Consequently, the Cr atom becomes vibrating faster [Fig. 1(a)], and the potential energy well becomes more symmetric [Fig. 3(d)]. Based on the above analysis of the coupling among electronic, magnetic and phononic properties, the weakened phonon anharmonicity and thus the enhanced thermal conductivity by spin-lattice coupling can be well understood from the fundamental point of view of electronic structure.

Before closing, we would like to point out that, the giant effect of spin-lattice coupling on the thermal transport discovered in this study is not limited to the case of 2D CrI_3. Similar phenomena could be also found in other systems, for example, the layered *van der Walls* magnetic materials in the 2D form, such as $CrGeTe_3$[31–33] and Fe_3GeTe_2,[34,35] (similar structure change as CrI_3 has been confirmed by our separate DFT calculation) which deserves further studies.

CONCLUSIONS

In summary, we performed first-principles study of spin effect on the geometric structure, lattice vibrations, and thermal transport in monolayer CrI_3. The struc- ture is found to be altered remarkably by the spin-lattice coupling, including lattice constant, bond angles, bond lengths, and atomic positions, which leads to the remarkably modulated thermal transport properties. The thermal conductivity of monolayer CrI_3 is enlarged more than two orders of magnitude by the spin-lattice coupling, which would be large enough for its applications in nanoelectronics and magnetic storage. The effect is found to be especially stronger for the acoustic phonon modes, which dominate thermal transport with FM ordering. Deep analysis shows that the mechanism lies in the spin-lattice coupling weakened phonon-phonon scattering due to the weakened phonon anharmonicity. Fundamental understanding on the underlying mechanism is achieved by analyzing the coupling among electronic, magnetic and phononic properties based on the orbital projected electronic structure and spin density. The Cr-Cr direct exchange and Cr-I-Cr superexchange induce additional strong interatomic interactions. Consequently, the structure becomes more symmetric with the lowered total energy of the system, and the Cr atom becomes vibrating faster, leading to the more symmetric potential energy well and the weakened phonon anharmonicity. To the best of our knowledge, for the first time this study uncovers the giant effect of spin-lattice coupling on the thermal transport properties with monolayer CrI_3 as a study case, which would deepen our understanding on thermal transport and shed light on future research of thermal transport in magnetic materials.

METHODS

All the first-principles calculations are performed based on the density functional theory (DFT) using the projector augmented wave (PAW) method[36] as implemented in the Vienna *ab initio* simulation package (vasp)[37]. The Perdew-Burke-Ernzerhof (PBE)[38] of generalized gradient approximation (GGA) is chosen as the exchange-correlation functional. The valence electron configurations of Cr and I atoms are considered as $p^6d^5s^1$ and s^2p^5, respectively. The kinetic energy cutoff of wave functions is set as 665 eV, and a Monkhorst-Pack[39] k-mesh of 15 × 15 × 1 is used to sample the Brillouin Zone (BZ), with the energy convergence threshold set as 10^{-6} eV. A large vacuum spacing of 20 A is employed along the *out-of-plane* direction. For the calculations of electronic, magnetic, and thermal transport properties of CrI_3 in FM state, we turn on the spin switch all the way, while switch off for the PM. The spin-orbit coupling is not included here. All geometries are fully optimized until the maximal Hellmann-Feynman force is smaller than 10^{-8} eV/A. The interatomic force constants (IFCs) are obtained based on the 4 × 4 × 1 supercell with convergence test performed. The phonon dispersions are evaluated based on the harmonic IFCs using the PHONOPY package[40]. The cutoff distance at the 9th nearest neighbors (~0.75 nm) is found to be large enough to obtain converged and reliable thermal conductivity[41]. During the procedure, the translational and rotational invariance of IFCs are enforced using the Lagrange multiplier method[40,42,43]. The Born effective charge (Z^*) and dielectric constant (E) are also included, which are obtained based on the density functional perturbation theory (DFPT). The interrogation grid in the thermal conductivity calculation is adopted as 70 × 70 × 1, which is chosen based on a full convergence test (Supplemen- tal Figure S2). The Gaussian broadening is set automatically in the calculations using an adaptive Gaussian broadening scheme so the method is completely parameter free. Finally, the thermal conductivity is obtained by solving the linearized phonon Boltzmann transport equation (BTE) using an iterative procedure as implemented in the ShengBTE package with the effective thickness of 7.09 A[43,44]. Detailed information on the employed methods can be found in Refs. [18,20,43–45].

ACKNOWLEDGMENTS

Simulations were performed with computing resources granted by RWTH Aachen University, Germany under

projects of rwth0366 and rwth0288. The numerical calculations in this paper have been done on the supercomputing system of the National Supercomputing Center in Changsha. H.W. is supported by the Na- tional Natural Science Foundation of China (Grant No. 51906097). Z.Q. is supported by the National Natural Science Foundation of China (Grant No. 11904324 and 11847158) and the China Postdoctoral Science Foundation (2018M642774). M.H. is supported by the NSF and SC EPSCoR/IDeA Program under NSF OIA-1655740 and SC EPSCoR/IDeA 19-SA06.

AUTHOR CONTRIBUTIONS

All authors researched, collated, and wrote this paper.

COMPETING INTERESTS

The authors declare no competing financial or non-financial interests.

DATA AVAILABILITY

The data that support this study are available from the corresponding author upon reasonable request.

* qin.phys@gmail.com; gzqin@hnu.edu.cn; Equal contribution
† Equal contribution
‡ qzz@zzu.edu.cn
§ hu@sc.edu

[1] Stockem, I. *et al.* Anomalous phonon lifetime shortening in paramagnetic CrN caused by spin-lattice coupling: A combined spin and *Ab Initio* molecular dynamics study. *Phys. Rev. Lett.* **121**, 125902 (2018). URL https://link.aps.org/doi/10.1103/PhysRevLett.121.125902.

[2] Burch, K. S., Mandrus, D. & Park, J.-G. Magnetism in two-dimensional van der waals materials. *Nature* **563**, 47–52 (2018). URL http://www.nature.com/articles/s41586-018-0631-z.

[3] Balandin, A. A. Thermal properties of graphene and nanostructured carbon materials. *Nat. Mater.* **10**, 569–581 (2011). URL http://dx.doi.org/10.1038/nmat3064.

[4] Huang, B. *et al.* Layer-dependent ferromagnetism in a van der waals crystal down to the monolayer limit. *Nature* **546**, 270–273 (2017). URL http://www.nature.com/doifinder/10.1038/nature22391.

[5] Liu, Y. & Petrovic, C. Anisotropic magnetocaloric effect in single crystals of CrI 3. *Phys. Rev. B* **97**, 174418 (2018). URL https://link.aps.org/doi/10.1103/PhysRevB.97.174418.

[6] Sivadas, N., Okamoto, S., Xu, X., Fennie, C. J. & Xiao, D. Stacking-dependent magnetism in bilayer CrI_3. *Nano Letters* **18**, 7658–7664 (2018). URL http://pubs.acs.org/doi/10.1021/acs.nanolett.8b03321.

[7] Wang, Z. *et al.* Very large tunneling magnetoresistance in layered magnetic semiconductor CrI3. *Nature Commun.* **9**, 2516 (2018). URL http://www.nature.com/articles/s41467-018-04953-8.

[8] Huang, B. *et al.* Electrical control of 2d magnetism in bilayer CrI3. *Nature Nanotechnology* **13**, 544–548 (2018). URL http://www.nature.com/articles/s41565-018-0121-3.

[9] Jiang, S., Shan, J. & Mak, K. F. Electric-field switching of two-dimensional van der waals magnets. *Nature Materials* **17**, 406–410 (2018). URL http://www.nature.com/articles/s41563-018-0040-6.

[10] Jiang, S., Li, L., Wang, Z., Mak, K. F. & Shan, J. Controlling magnetism in 2d CrI3 by electrostatic doping. *Nature Nanotechnology* **13**, 549–553 (2018). URL http://www.nature.com/articles/s41565-018-0135-x.

[11] Webster, L. & Yan, J.-A. Strain-tunable magnetic anisotropy in monolayer $CrCl_3$, $CrBr_3$, and CrI_3. *Phys. Rev. B* **98**, 144411 (2018). URL https://link.aps.org/doi/10.1103/PhysRevB.98.144411.

[12] Wang, H., Fan, F., Zhu, S. & Wu, H. Doping enhanced ferromagnetism and induced half-metallicity in CrI3 monolayer. *EPL (Europhysics Letters)* **114**, 47001 (2016). URL https://iopscience.iop.org/article/10.1209/0295-5075/114/47001/meta.

[13] Wu, Z., Yu, J. & Yuan, S. Strain-tunable magnetic and electronic properties of monolayer CrI_3. *Physical Chemistry Chemical Physics* **21**, 7750–7755 (2019). URL http://xlink.rsc.org/?DOI=C8CP07067A.

[14] Larson, D. T. & Kaxiras, E. Raman spectrum of CrI 3 : An ab initio study. *Physical Review B* **98**, 085406 (2018). URL https://link.aps.org/doi/10.1103/PhysRevB.98.085406.

[15] Jiang, J.-W. Phonon bandgap engineering of strained monolayer MoS2. *Nanoscale* **6**, 8326–8333 (2014). URL http://dx.doi.org/10.1039/C4NR00279B.

[16] Qin, G., Qin, Z., Yue, S.-Y., Yan, Q.-B. & Hu, M. External electric field driving the ultra-low thermal conductivity of silicene. *Nanoscale* **9**, 7227–7234 (2017). URL http://dx.doi.org/10.1039/C7NR01596H.

[17] Plata, J. J. *et al.* An efficient and accurate framework for calculating lattice thermal conductivity of solids: AFLOWAAPL automatic anharmonic phonon library. *npj Computational Materials* **3**, 45 (2017). URL http://www.nature.com/articles/s41524-017-0046-7.

[18] Qin, G. *et al.* Resonant bonding driven giant phonon anharmonicity and low thermal conductivity of phosphorene. *Phys. Rev. B* **94**, 165445 (2016). URL http://link.aps.org/doi/10.1103/PhysRevB.94.165445.

[19] Qin, G. & Hu, M. Thermal transport in phosphorene. *Small* **14**, 1702465 (2018). URL https://onlinelibrary.wiley.com/doi/abs/10.1002/smll.201702465.

[20] Qin, Z., Qin, G., Zuo, X., Xiong, Z. & Hu, M. Orbitally driven low thermal conductivity of monolayer gallium

nitride (gan) with planar honeycomb structure: a comparative study. *Nanoscale* **9**, 4295–4309 (2017). URL http://dx.doi.org/10.1039/C7NR01271C.

[21] Qin, G., Qin, Z., Wang, H. & Hu, M. Anomalous- ly temperature-dependent thermal conductivity of monolayer gan with large deviations from the traditional $1/t$ law. *Phys. Rev. B* **95**, 195416 (2017). URL https://link.aps.org/doi/10.1103/PhysRevB.95.195416.

[22] Qin, G., Qin, Z., Wang, H. & Hu, M. Lone-pair electrons induced anomalous enhancement of thermal transport in strained planar two-dimensional materials. *Nano Energy* **50**, 425–430 (2018). URL http://www.sciencedirect.com/science/article/pii/S2211285518303574.

[23] Burch, K. S. Electric switching of magnetism in 2d. *Nature Nanotechnology* **13**, 532–532 (2018). URL http://www.nature.com/articles/s41565-018-0165-4.

[24] Broido, D. A., Ward, A. & Mingo, N. Lattice thermal conductivity of silicon from empirical interatomic potentials. *Phys. Rev. B* **72**, 014308 (2005). URL http://link.aps.org/doi/10.1103/PhysRevB.72.014308.

[25] Lindsay, L., Broido, D. A. & Reinecke, T. L. First-principles determination of ultrahigh thermal conductivity of boron arsenide: A competitor for diamond? *Phys. Rev. Lett.* **111**, 025901 (2013). URL http://link.aps.org/doi/10.1103/PhysRevLett.111.025901.

[26] Peng, B. *et al.* Phonon transport properties of two-dimensional group-IV materials from *ab initio* calculations. *Physical Review B* **94**, 245420 (2016). URL https://link.aps.org/doi/10.1103/PhysRevB.94.245420.

[27] Seyler, K. L. *et al.* Ligand-field helical luminescence in a 2d ferromagnetic insulator. *Nature Physics* **14**, 277–281 (2018). URL http://www.nature.com/articles/s41567-017-0006-7.

[28] Qin, Z., Xiong, Z., Qin, G. & Chen, L. Energetics and magnetism of co-doped GaN(0001) surfaces: A first-principles study. *J. Appl. Phys.* **116**, 224503 (2014). URL http://aip.scitation.org/doi/10.1063/1.4904055.

[29] McGuire, M. A., Dixit, H., Cooper, V. R. & Sales, B. C. Coupling of crystal structure and magnetism in the layered, ferromagnetic insulator CrI_3. *Chemistry of Materials* **27**, 612–620 (2015). URL http://pubs.acs.org/doi/10.1021/cm504242t.

[30] Lin, G. T. *et al.* Critical behavior of two-dimensional intrinsically ferromagnetic semiconductor CrI_3. *Appl. Phys. Lett.* **112**, 072405 (2018). URL http://aip.scitation.org/doi/10.1063/1.5019286.

[31] Gong, C. *et al.* Discovery of intrinsic ferromagnetism in two-dimensional van der waals crystals. *Nature* **546**, 265–269 (2017). URL http://www.nature.com/articles/nature22060.

[32] Li, Y. F. *et al.* Electronic structure of ferromagnetic semiconductor CrGeTe 3 by angle-resolved photoemission spectroscopy. *Phys. Rev. B* **98**, 125127 (2018). URL https://link.aps.org/doi/10.1103/PhysRevB.98.125127.

[33] Lin, G. T. *et al.* Tricritical behavior of the two-dimensional intrinsically ferromagnetic semiconductor CrGeTe 3. *Phys. Rev. B* **95**, 245212 (2017). URL http://link.aps.org/doi/10.1103/PhysRevB.95.245212.

[34] Fei, Z. *et al.* Two-dimensional itinerant ferromagnetism in atomically thin fe3gete2. *Nature Materials* **17**, 778–782 (2018). URL http://www.nature.com/articles/s41563-018-0149-7.

[35] Johansen, y., Risinggrd, V., Sudb, A., Linder, J. & Brataas, A. Current control of magnetism in two-dimensional fe 3 GeTe 2. *Phys. Rev. Lett.* **122**, 217203 (2019). URL https://link.aps.org/doi/10.1103/PhysRevLett.122.217203.

[36] Kresse, G. & Joubert, D. From ultrasoft pseudopotentials to the projector augmented-wave method. *Phys. Rev. B* **59**, 1758–1775 (1999). URL http://link.aps.org/doi/10.1103/PhysRevB.59.1758.

[37] uller, J. Efficient iterative schemes for ab initio total-energy calculations using a plane-wave basis set. *Phys. Rev. B* **54**, 11169–11186 (1996). URL http://link.aps.org/doi/10.1103/PhysRevB.54.11169.

[38] Perdew, J. P., Burke, K. & Ernzerhof, M. Generalized gradient approximation made simple. *Phys. Rev. Lett.* **77**, 3865–3868 (1996). URL http://link.aps.org/doi/10.1103/PhysRevLett.77.3865.

[39] Monkhorst, H. J. & Pack, J. D. Special points for brillouin-zone integrations. *Phys. Rev. B* **13**, 5188–5192 (1976). URL http://link.aps.org/doi/10.1103/PhysRevB.13.5188.

[40] Togo, A., Oba, F. & Tanaka, I. First-principles calculations of the ferroelastic transition between rutile-type and $CaCl_2$-type SiO_2 at high pressures. *Phys. Rev. B* **78**, 134106 (2008).

[41] Qin, G. & Hu, M. Accelerating evaluation of converged lattice thermal conductivity. *npj Computational Materials* **4**, 3 (2018). URL https://doi.org/10.1038/s41524-017-0058-3.

[42] Esfarjani, K. & Stokes, H. T. Method to extract anharmonic force constants from first principles calculations. *Phys. Rev. B* **77**, 144112 (2008). URL http://link.aps.org/doi/10.1103/PhysRevB.77.144112.

[43] Li, W., Lindsay, L., Broido, D. A., Stewart, D. A. & Mingo, N. Thermal conductivity of bulk and nanowire $Mg_2Si_xSn_{1-x}$ alloys from first principles. *Phys. Rev. B* **86**, 174307 (2012). URL http://link.aps.org/doi/10.1103/PhysRevB.86.174307.

[44] Li, W., Carrete, J., Katcho, N. A. & Mingo, N. Shengbte: A solver of the boltzmann transport equation for phonons. *Comput. Phys. Commun.* **185**, 1747–1758 (2014). URL http://www.sciencedirect.com/science/article/pii/S0010465514000484.

[45] Qin, G. *et al.* Diverse anisotropy of phonon transport in two-dimensional group IV-VI compounds: A comparative study. *Nanoscale* **8**, 11306–11319 (2016). URL http://dx.doi.org/10.1039/C6NR01349J.